JGR Solid Earth

RESEARCH ARTICLE
10.1029/2018JB017204

The Benefits of Using a Network of Superconducting Gravimeters to Monitor and Study Active Volcanoes

Daniele Carbone[1], Flavio Cannavò[1], Filippo Greco[1], Richard Reineman[2], and Richard J. Warburton[2]

[1]Istituto Nazionale di Geofisica e Vulcanologia, Sezione di Catania - Osservatorio Etneo, Catania, Italy, [2]GWR Instruments, Inc., San Diego, California, USA

Key Points:
- Continuous volcano gravimetry can be accomplished with SGs that provide higher quality data than the more widely used spring meters
- A great care must be paid to hydrological processes that can induce gravity changes with amplitude comparable to volcano-related anomalies
- SGs can detect volcano-related gravity changes that would otherwise stay hidden, thus providing unique information on the driving processes

Supporting Information:
- Supporting Information S1

Correspondence to:
D. Carbone,
daniele.carbone@ingv.it

Citation:
Carbone, D., Cannavò, F., Greco, F., Reineman, R., & Warburton, R. J. (2019). The benefits of using a network of superconducting gravimeters to monitor and study active volcanoes. *Journal of Geophysical Research: Solid Earth*, *123*. https://doi.org/10.1029/2018JB017204

Received 18 DEC 2018
Accepted 12 MAR 2019
Accepted article online 15 MAR 2019

Abstract We present results from a mini-array of three iGrav superconducting gravimeters (SGs) at Mount Etna. This is the first network of SGs ever installed on an active volcano. Continuous gravity measurements at active volcanoes are mostly accomplished with spring gravimeters that can be operated even under harsh field conditions. Nevertheless, these instruments do not provide reliable continuous measurements over periods longer than a few days due to the instrumental drift and artifacts driven by ambient parameters. SGs are free from these instrumental effects and thus allow to track even small gravity changes (1–2 μGal) over a wide range of time scales (minutes to months). However, SGs need host facilities with main electricity and a large installation surface, implying that they cannot be deployed in close proximity to the active structures of tall volcanoes. At Mount Etna the three iGrav SGs were installed at distances from the summit active craters ranging between 3.5 and 15 km. Despite the relatively unfavorable position of the installation sites, we show that these instruments can detect meaningful (i.e., volcano-related) changes that would otherwise remain hidden, like, for example, the weak gravity signature (within a few μGal) of gas buildup at intermediate depth in the plumbing system of Etna, during noneruptive intervals. Our results prove that iGrav SGs are powerful tools to monitor and study active volcanoes and can provide unique information on the bulk processes driving volcanic activity.

1. Introduction

Among the parameters that are used to monitor and study active volcanoes (Tilling, 2008), gravity has a great potential, since it is the only measurable quantity directly related to mass (density) changes at depth. Past studies have demonstrated that gravimetry can supply unique information on the process driving volcanic activity (Battaglia et al., 2008; Carbone et al., 2017). For example, if gravity data are analyzed jointly with other information (e.g., ground deformation and seismicity), it is possible to set constraints on the density of the intruding fluid, thus distinguishing whether a phase of unrest is driven by magma, gas, or hydrothermal fluids (e.g., Battaglia et al., 2003, 2006). This information is important given its implications on hazard assessment.

Gravity changes driven by volcanic processes occur over a wide range of time scales, from minutes to years. Accordingly, both time-lapse surveys, along networks of stations, and continuous measurements at single points are accomplished. Time-lapse observations have been performed at several volcanoes during the last 4 decades, providing insight into the processes underlying volcanic activity that could not be gained using other techniques (see Battaglia et al., 2008, and references therein). The repetition time of the surveys, in most cases longer than a few months, dictates that only changes occurring over time scales of several months to years can be observed (Carbone et al., 2017). Conversely, continuous gravity measurements, able to image processes over short time scales (down to minutes), have not been widely applied to increase understanding about the processes operating during volcanism. Continuous volcano gravimetry is mostly accomplished with spring gravimeters that are relatively compact and small (thus easily portable) and can be operated on DC power, thus allowing installation in remote sites, that is, close to active craters, where the instrumentation is run on solar panels and batteries (e.g., Carbone et al., 2015). When used in continuous mode, spring gravimeters do not usually provide reliable measurements over periods longer than a few days. Indeed, past studies have shown that the combined effect of instrumental drift and environmental factors (mostly, ambient temperature) may induce strong apparent gravity changes that are difficult to predict since highly nonlinear, instrument-specific, and frequency-dependent modeling schemes are required (Andò &

Carbone, 2004). If a suitable setup is adopted for the field stations, these effects become negligible over short intervals, which explains why most past studies at active volcanoes have focused on the analysis of continuous gravity observations over time scales of minutes to a few days (e.g., Branca et al., 2003; Carbone et al., 2006, 2008, 2009, 2012, 2015; Carbone & Poland, 2012; Gottsmann et al., 2007; Poland & Carbone, 2016, 2018; Sainz-Maza Aparicio et al., 2014).

Superconducting gravimeters (SGs; Goodkind, 1999; Hinderer et al., 2015) provide an alternative to spring instruments for continuous observations at volcanoes. Instead of a mechanical spring, SGs employ the magnetic levitation of a superconducting Niobium sphere in a field of superconducting persistent coils. By utilizing the perfect stability of supercurrents, a completely reliable, nonmechanical spring is created (Goodkind, 1999). SGs thus yield higher-quality data than spring instruments. Indeed, they are unaffected by ambient parameters and feature sub-μGal precision (0.05 μGal over 1-min averaging; 1 μGal = 10^{-8} ms^{-2}) and negligible instrumental drift (<0.5 μGal/month; for comparison, the typical drift of spring gravimeters is on the order of 10^3 μGal/month). Hence, SGs allow to track even small gravity changes (on the order of 1–2 μGal) over a wide range of time scales (minutes to months). However, since the superconducting state is reached at very low temperatures (<9.2 K), the SG sensor is operated inside a dewar filled with liquid helium and the equipment must include a cryogenic refrigerator (compressor and coldhead) and the helium tank. Hence, even in the case of the most compact SG, the iGrav by GWR (Warburton et al., 2010), the facility that hosts the instrumentation must have an installation surface of at least 2 m^2 and, since the compressor requires ~1.4 kW of power, it must be supplied with main electricity. Installation sites with these characteristics are hardly found in the summit zones of tall volcanoes (i.e., close to the active craters). Given their high precision and long-term stability, SGs can detect meaningful signals even if they are not placed in close proximity to the active structures. The above observations, coupled to the high cost of these instruments, dictate that the choice to install an SG—or a SG network—at a volcano must be subordinated to a careful feasibility study, aimed at verifying that the candidate installation sites are suitably located to ensure that volcano-related changes are likely to be detectable.

2. The Mini-Array of iGrav SGs at Mount Etna

The installation of iGrav SGs at Mount Etna began in 2014, in the framework of an infrastructural project (VULCAMED) funded by the European Community and by Italian national sources. This is the first network of SGs ever installed on an active volcano.

In September 2014, iGrav#16 was installed in the facilities of the Serra La Nave Astrophysical Observatory (SLN; 1,730 m above sea level (asl); ~6.5 km from the summit craters; Figure 1), managed by the Italian National Institute for Astrophysics.

In the summer of 2016, iGrav#20 and iGrav#25 were also installed on Etna. The installation site of iGrav#20 is currently the highest site on Etna where electricity is available: La Montagnola hut (MNT; 2,600 m asl; ~3.5 km SE of the summit craters; Figure 1). This facility also hosts thermal and visible cameras in the monitoring network of INGV-OE (www.ct.ingv.it). The installation of iGrav#20 at La Montagnola was especially challenging; the air-cooled compressor needs the environmental protection of the hut, but its exhaust heat would rapidly overheat the interior of the small hut. We solved this problem by attaching a large-diameter plastic corrugated pipe to the compressor output, to direct the hot air through an outlet duct in the wall, while a second inlet duct allows air to return from the outside. Additional fans were added to force the hot air out. This “heat discharge system” prevents the ambient room temperature from rising too much, especially during the warmer seasons.

iGrav#25 was installed in the facilities of INGV-OE located in the village of Nicolosi (NIC; 720 m asl; ~15 km SE of the summit craters; Figure 1). Owing to the long distance from the active craters of Etna, the signal from NIC is not supposed to be relevantly affected by gravity changes driven by volcanic processes. Hence, this signal is mainly used to recognize, in the time series from the other two SGs, changes that (i) are not volcano-related and (ii) are not accounted for by the standard corrections applied to the gravity data. The latter include corrections for the effect of Earth tides (Wenzel, 1996), local atmospheric pressure variations (Merriam, 1992), and polar motion (Hinderer et al., 2015).

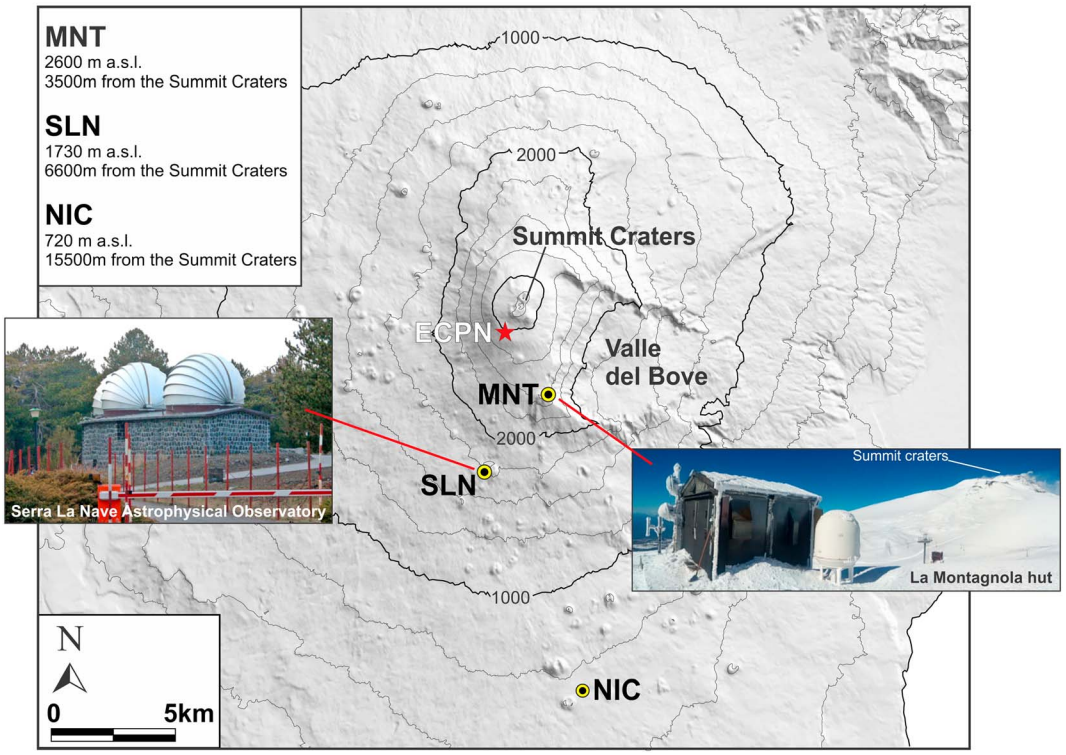

Figure 1. Sketch map of Mount Etna showing the position of the three stations equipped with iGrav SGs. The red star marks the position of ECPN seismic station. The inset at the top right shows the active craters in the summit zone of Etna. The yellow dot marks the position of the new vent that opened on December 2016 within the Southeast Crater Complex (SECC). The two photos show the facilities housing the instrumentation at SLN and MNT stations.

The noise levels of iGrav#16 (SLN), iGrav#20 (MNT), and iGrav#25 (NIC) are reported in Figure 2 (black, red, and blue curves, respectively), which shows for each instrument, the PSD averaged over three quiet days (PSDs are calculated using Welch's averaged periodgram method). The "new low-noise model" (Peterson, 1993) is also reported in Figure 2 (dashed purple line) for reference. The noise level at NIC and SLN is only slightly higher than that observed in nonvolcanic sites (e.g., Rosat & Hinderer, 2018; Van Camp et al., 2017;

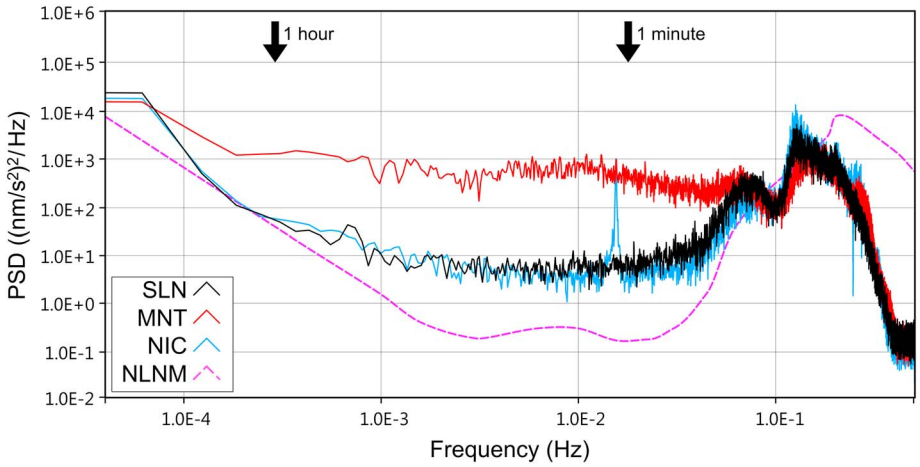

Figure 2. Power spectral densities (PSD) of the gravity signals from SLN, MNT, and NIC (black, red, and blue curves, respectively), averaged over three quiet days. The "new low-noise model" (NLNM) is also shown (dashed purple curve). The peak in the PSD of the signal from NIC denotes a mode (~65 s) of the proof-sphere that is almost always excited at the installation site.

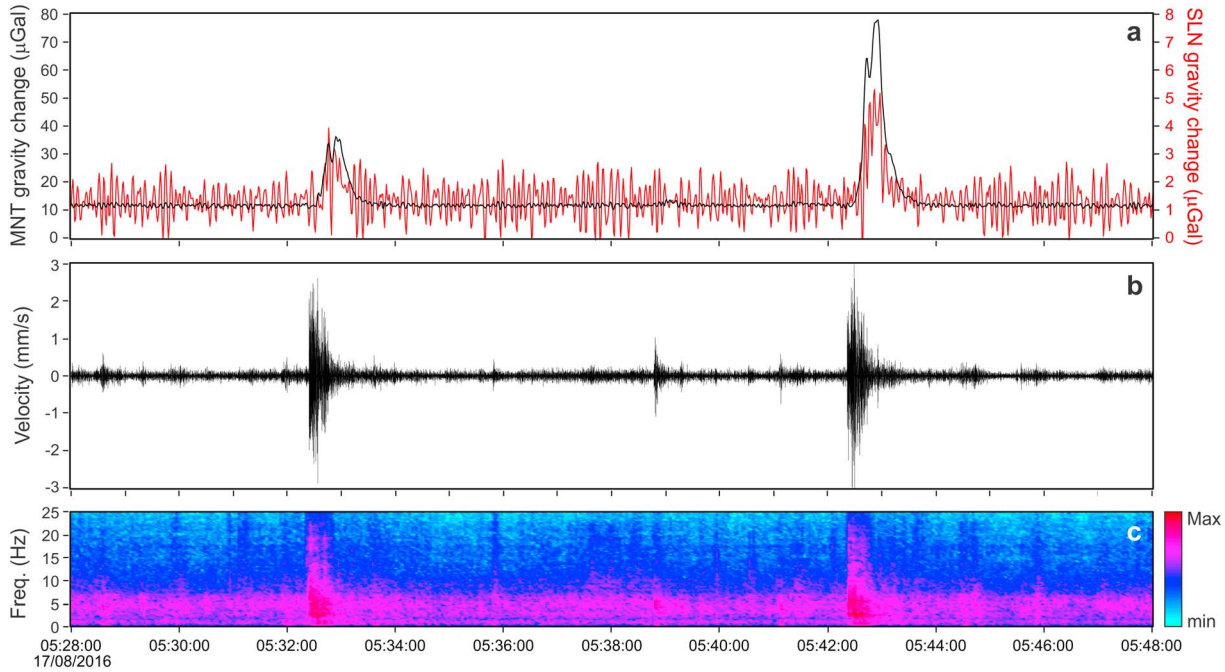

Figure 3. (a) Positive anomalies in the gravity signal from MNT (black curve) and SLN (red curve). These anomalies occur in correspondence of long-period seismic events. (b) Seismic velocity along the horizontal (EW) direction, observed at a site (ECPN; 2,990-m elevation; see Figure 1), ~1 km away from the summit craters of Etna. (c) Spectrogram of the signal in (b).

Warburton et al., 2010). At MNT the noise level is up to 15 times higher than at NIC and SLN, over the frequency band of 10 mHz to 0.1 Hz. This is due to the higher level of volcano-related seismic noise at the station that is nearest to the summit active zone of Etna (Figure 1). Nonetheless, we demonstrate that is still possible to monitor gravity changes of a few μGal at MNT (see section 5).

In some cases, the shaking due to seismic waves from volcanic activities also triggers positive changes in the average level of the gravity signal from MNT. Indeed, positive anomalies with amplitude ranging between a few and a few tens of μGal were found to occur over time scales of 30 to 60 s (Figure 3a), each associated to a long-period seismic event (Figures 3b and 3c). This effect is due to the horizontal forces from seismic shaking that push the proof sphere of the iGrav off to the side. Since the levitation force gets weaker as the sphere moves off the axis of the magnet coils, the sphere drops, thus simulating an increase in gravity. On some occasions, these instrumental effects are also observed at SLN, but with an amplitude more than 1 order of magnitude smaller than at MNT (Figure 3a). The smaller amplitude is likely due to the longer distance to the active structures in the summit zone of the volcano (Figure 1). The same kind of instrumental effect is also produced during phases of strong volcanic tremor amplitude (e.g., intervals when strong Strombolian and fountaining activity takes place) that are often accompanied by sudden increases in the average level of the gravity signal (Figure 4). It is very important to identify, especially in the signal from the station at higher elevation, these instrumental effects, thus distinguishing real changes, driven by gravity acceleration, from (apparent) changes resulting from the instrumental response to inertial forces (Carbone et al., 2010).

3. Hydrological Effects on the Gravity Time Series From Etna

Previous studies showed that changes in groundwater mass may induce gravity changes measurable at the surface, over a wide range of time scales (hours to years; Creutzfeldt et al., 2008). This effect can reach a few to a few tens of μGal (Güntner et al., 2017; Hemmings et al., 2016) and should be removed from the observed time series to retrieve the gravity changes due to volcanic processes. Nevertheless, simulating the contribution of groundwater to observed gravity changes is not an easy task, since several overlapping components affect the water balance, including precipitation (both rainfall and snowfall), evapotranspiration (Van Camp et al., 2016), and water runoff from the storage beneath the installation site. Beside water

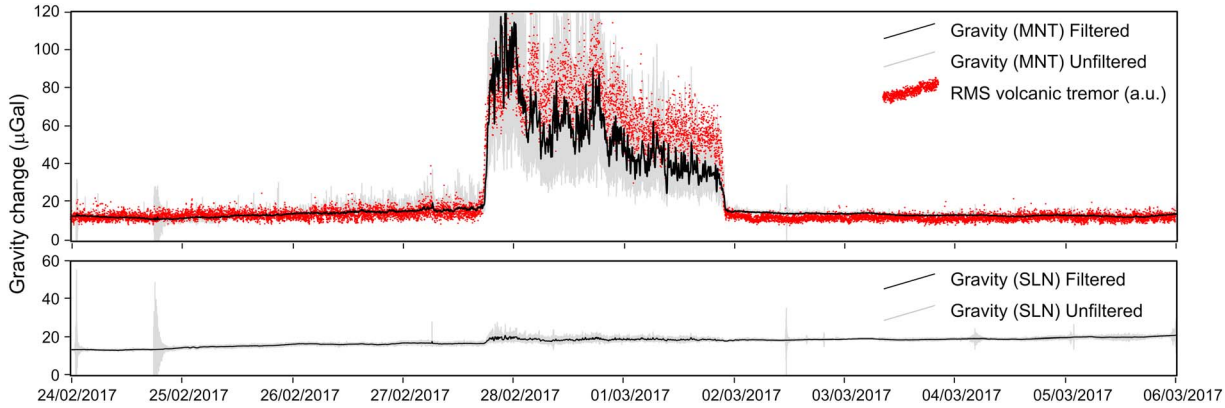

Figure 4. (top) Apparent positive gravity changes observed at MNT and induced by ground shaking from strong volcanic tremor. Data are corrected for the effects of Earth tides and local atmospheric pressure changes. Gray curve: unfiltered gravity signal; black curve: low-pass-filtered gravity signal, with cutoff frequency of 10 mHz; red-dotted curve: root-mean-square (RMS) amplitude of the vertical component of the seismic signal, recorded by a station in the summit zone of Etna. (bottom) Gravity signal observed at SLN during the same interval (same vertical scale). Gray and black curves are as in the top chart.

table fluctuations, changes in water-mass storage above the water table, that is, within the unsaturated (vadose) zone, must be taken into account when evaluating the hydrological component of the gravity signal. Under some circumstances, the latter component may induce most of the water-related gravity effect, that is, in areas where, due to a combination of high permeability and high relief, the vadose zone is relatively thick (Hemmings et al., 2016).

The installation sites of the three iGra versus on Etna (Figure 1) have different characteristics and different types of gravity responses to hydrological effects are expected at each of them. While iGrav#25, in the village of Nicolosi (NIC station; Figure 1), is surrounded, to some hundreds of meters, by an almost flat land, with sealed surfaces of roads and buildings, iGrav#20, at MNT station (Figure 1), is installed inside a mountain shelter with a small footprint (~25 m^2). The latter is surrounded by steep topography, with land cover mostly consisting of volcanic ash and lava flows. Between these two extremes, iGrav#16, in the facilities of SLN Astrophysical Observatory (Figure 1), is housed in a building with an ~250-m^2 footprint. Topography in the surroundings of the observatory is almost flat and land cover is given by a mosaic of grassland, forest, and sealed surfaces (roads and buildings).

The available time series from SLN covers an interval of nearly three years (October 2014–August 2017; Figure 5a), while those from both MNT and NIC cover the period from July 2016 to August 2017 (slightly more than 1 year; Figures 5b and 5c). Hence, the time series acquired at SLN is the most suitable to study seasonal components of the groundwater effect on gravity. This time series is dominated by two strong increases occurring during February–April 2015 and February–April 2017, respectively. A comparison with the amount of snow accumulation at SLN (Figure 5d), evaluated through GNSS reflectometry (Larson & Nievinski, 2013; see supporting information), using the signal from ESLN GPS station (only 30 m from the installation site of iGrav#16), shows that both increases occurred during phases of snow melting. Hence, they are likely due to rapid increases in groundwater mass. As shown in Figure 5a, a similar increase did not occur in 2016. Indeed, much less snow fell that year, than in 2015 and 2017 (Figure 5d). Besides snowfall data, rainfall data are also available for the installation site of iGrav#16 (Figure 5e), owing to the meteorological station managed by Italian National Institute for Astrophysics at the SLN Astrophysical Observatory.

Following the empirical method of Crossley et al. (1998), we calculate the gravity effect due to changes in groundwater mass as

$$g(t) = K_{hg} \cdot w(t-t_0) \cdot \left(1-e^{-\frac{t-t_0}{\tau_1}}\right)\left(e^{-\frac{t-t_0}{\tau_2}}\right) \quad (1)$$

where K_{hg} is the sensitivity factor to convert water storage fluctuations into corresponding gravity changes (under the Bouguer slab approximation, K_{hg} has a value of about 42 μGal/m); $w(t - t_0)$ is the cumulative amount of precipitation during the interval between t_0 and t; and τ_1 and τ_2 are the charge and discharge

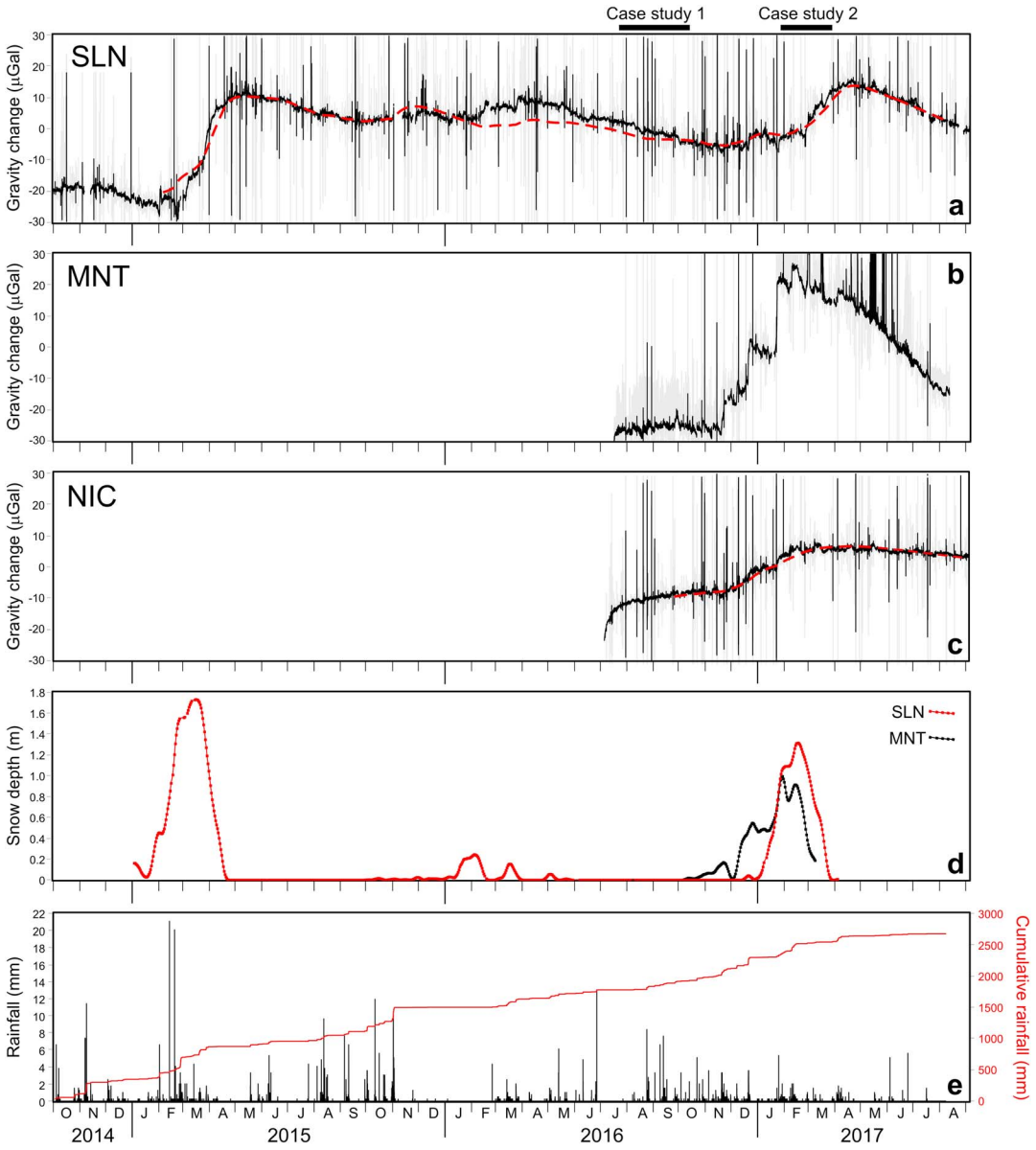

Figure 5. (a) Gravity signal observed at SLN station through iGrav#16 SG, during October 2014 to August 2017. Data are corrected for the effects of Earth tides, local atmospheric pressure changes, and polar motion (gray curve: unfiltered signal; black curve: low-pass filtered signal, with cutoff frequency of 10 mHz). The dashed red curve is the modeled time series of the gravity effect induced by water-mass changes (see text for details). (b) Gravity signal observed at MNT station through iGrav#20 SG, during July 2016 to August 2017 (gray and black curves as in (a)). (c) Gravity signal observed at NIC station through iGrav#25 SG, during July 2016 to August 2017 (gray, black, and dashed red curves as in (a)). (d) Changes in snow depth calculated through the GNSS reflectometry method at two sites 30 m (red curve) and 500 m (black curve) from SLN and MNT, respectively. (e) Ten-minute precipitation rates and cumulative rainfall observed at SLN, during October 2014 and August 2017.

times, that is, the time constants for infiltration toward and release from the storage beneath the observation point. $w(t - t_0)$ accounts for both rain and snow. To convert the snow depth changes into equivalent quantity of liquid water, a compactness coefficient of snow (K_{sw}) must be considered, that, usually, for fresh snow, is in the range of 5–30% (Judson & Doesken, 2000). Note that only negative variation of snow depth (snow melting) are considered in equation (1).

Indeed, since topography in the surroundings of the installation site is almost flat, snow accumulation occurs on the same horizon as the observation point, implying a negligible effect on the vertical component of the gravity acceleration. By knowing the overall water input, we can calculate the time series of the induced gravity effect (equation (1)) and compare it with the observed gravity to recognize components

Table 1
Best Fitting Parameters (See Text for Details) using Equation (1) and Gravity Data From SLN and NIC

	τ_1 (days)	τ_2 (days)	K_{hg} (μGal/m)	K_{sw}	Correlation Coefficient	RMS (μGal)
SLN	21	258	38	0.34	0.88	3.64
NIC	25	301	37	-	0.95	1.94

driven by redistribution of underground water mass. To invert the unknown parameters (τ_1, τ_2, K_{hg}, K_{sw}), we utilize a nonnegative constrained nonlinear optimization algorithm (i.e., Waltz et al., 2006) that is aimed at minimizing the root-mean-square difference between observed and modeled time series of gravity. The first part of the time series is excluded from the evaluation of the objective function. Indeed, since rainfall data prior to September 2014 are not available, bias could arise from not considering the discharge of groundwater from unknown rainfall. We choose to exclude the first ~100 days of the time series, as a compromise between disregarding the discharge effect of previous rain events, while taking into account the recharge due to strong rain events and snow melting during February to April 2015 (Figures 5d and 5e). Search ranges are set for K_{hg} and K_{sw}, to avoid convergence toward unrealistic values.

The values of τ_1 and τ_2 (21 and 258 days; Table 1), obtained from the optimization procedure, indicate relatively fast water infiltration, likely through fractured lavas, and the presence of a low-permeability "barrier" that retards the outward movement of water from the aquifer. The values of K_{hg} (38 μGal/m) is lower than expected from the infinite slab model, likely because the aquifer has a finite, rather than infinite, lateral extension (Mouyen et al., 2016). The modeled gravity time series (dashed line in Figure 5a) reproduces most of the observed changes (correlation coefficient = 0.88). However, some discrepancies are found, which could indicate either (i) the occurrence of gravity changes not driven by hydrological processes, or (ii) the inadequacy of the adopted model to accurately reproduce the gravity effect of groundwater changes at SLN, or (iii) that some key parameters are not sufficiently constrained (e.g., uncertainty on the data provided by the rain gauge due to wind and evaporation effects, errors on the amount of snow accumulation due to intrinsic limitations of the GNSS reflectometry method). It is also important to stress that due to the lack of data, evapotranspiration (Van Camp et al., 2016) is not accounted for by the model.

A similar calculation is performed using data from NIC; in this case, $w(t - t_0)$ only accounts for rain (NIC is at lower elevation than SLN and snow does not significantly contribute to the water-mass balance). Rainfall data are provided by Servizio Informativo Agrometeorologico Siciliano (www.sias.regione.sicilia.it) for a site 4 km from NIC and at about the same elevation. We cannot apply the above-described inversion procedure due to the relatively short duration of the time series from NIC (less than 1 year) and to the small amplitude of the water-driven gravity changes. Indeed, the algorithm does not converge stably, since a wide range of input parameters leads to identical solutions. Therefore, we perform a direct calculation to evaluate the fit of the observed gravity signal to the predictive model. We estimate that, assuming values of τ_1 and τ_2 similar to (yet sensibly higher than) those found using data from SLN, the predicted and observed gravity time series (dashed and solid lines in Figure 5c) agree remarkably well (Table 1), especially over the long-term components (correlation coefficient = 0.95). This result suggests that similar structural conditions control underground water transmission at SLN and NIC.

The time sequence acquired at MNT since July 2016 (Figure 5b) does not exhibit a long-term pattern coherent with observations from SLN and NIC. Rather, several sudden changes (over periods of a few hours to a few days) are observed in the gravity signal from MNT. Rainfall data from the close surroundings of MNT are not available. However, it appears that most of the above steps took place simultaneously with rainfall events at SLN, even though the gravity signals induced by the rainfall at SLN are either not present or exhibit a much lower amplitude than the gravity signals observed at MNT (Figure 6).

The above observations suggest that similar patterns of hydrological input (the two sites are less than 4 km apart) induce different gravity responses at SNL and MNT due to site effects. In other words, gravity changes due to hydrogeological processes at greater depth are less evident at MNT, being masked by local effects, such as water content variations in the shallowest ash layers beneath the observation point (Hemmings et al., 2016). Furthermore, the steep topography around MNT amplifies the gravity effect of shallow water storage variations. Using a numerical model with a prism approximation (e.g., Carbone et al., 2013), where the elevation of each prism with respect to the observation point is defined through a 5-m resolution DEM, we calculate the gravity effect of water storages within layers that are parallel to the ground surface and are located at different depths (top at 2 to 10 m from the surface). The overall gravity effect at the observation point is calculated by summing up the gravity effects induced by the water mass changes in each prism.

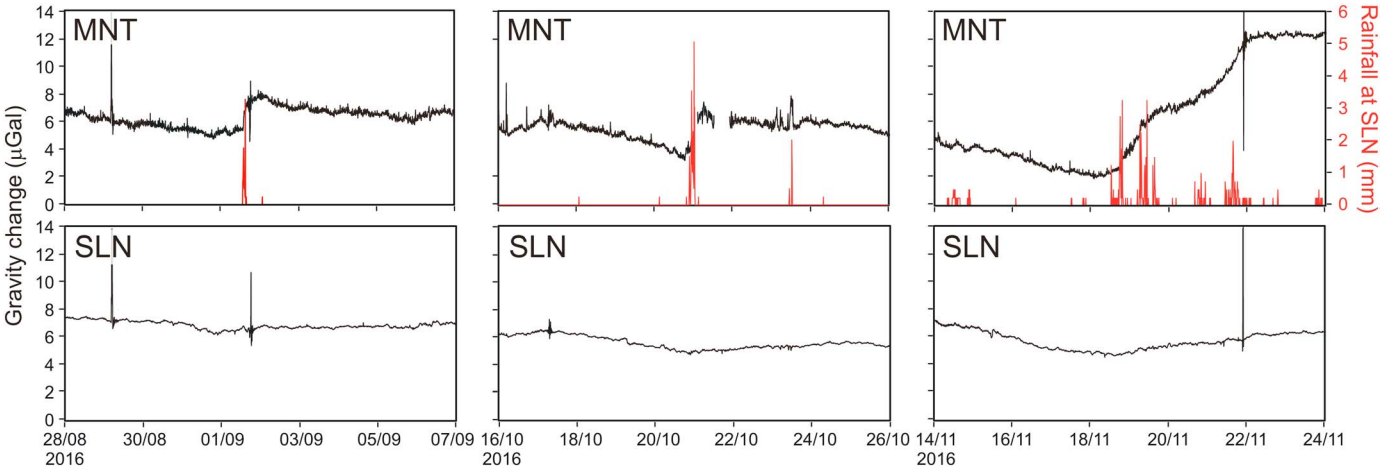

Figure 6. Three examples of rainfall events inducing short-time scale changes at MNT and almost no change at SLN. (top charts) Black curves:gravity signal from MNT corrected for the effects of Earth tides and local atmospheric pressure changes. Data are low-pass filtered with cutoff of 10 mHz. Red curves: 10-min precipitation rates observed at SLN. (bottom charts) Gravity signal from SLN (same corrections and same filter as for the gravity signal in the top charts).

As shown in Figure 7, assuming an increasingly higher integration radius around the observation point, the gravity effect of the water mass storage at different depths tends asymptotically to a value higher than that predicted by the Bouguer slab approximation. It is also important to stress that the "umbrella effect," that is, the effect of the building housing the gravimeter on the distribution of shallow water storage changes (Deville et al., 2013), is negligible at MNT due to the small footprint of the housing building. This is a further reason why the gravity effect of local water content variations in the unsaturated zone is expected to be relevant at MNT.

The evaluation of the gravity effect induced by groundwater mass changes at MNT would thus require a more complex model, than at SLN and NIC, considering the strong contribution of water-mass storage fluctuations in the uppermost unsaturated zone that overwhelms the effect of water table changes at greater depth (Deville et al., 2013). Due to lack of relevant information (e.g., local rainfall data), we do not consider as appropriate the application of a such model to the whole time series from MNT. Indeed, preliminary tests we carried out show that results obtained using rainfall data from SLN are not satisfactory, probably due to relevant differences in the amount of rain that falls on the two sites during the same rain event (the two sites are separated by a relatively short distance, but the difference in elevation is as high as 860 m). As detailed in section 5, a calculation is performed to model the effect of water-mass changes on the signal from MNT over

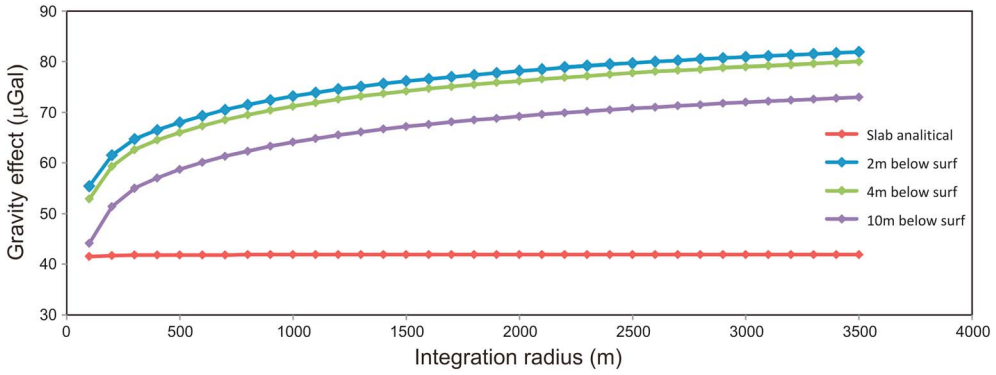

Figure 7. Simulated gravity effect, at MNT station, of 1-m-thick water storages confined within layers that are parallel to the ground surface. The tops of the water layers are at 2 (blue curve), 4 (green curve), and 10 m (purple curve) below the ground surface. Numerical calculations are performed at different integration radii around the observation point (up to 3.5 km). The red curve indicates the analytically derived effect of an infinite water slab (Bouguer approximation; same thickness).

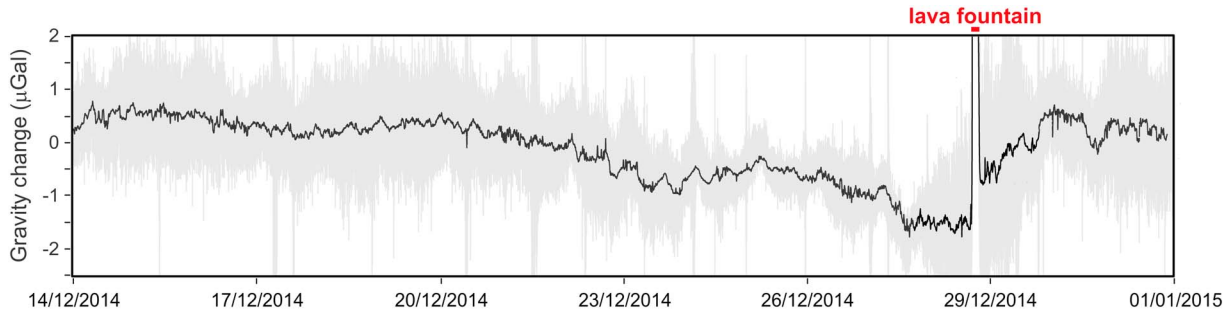

Figure 8. Gravity changes observed at SLN station before and after the lava fountaining episode on 28 December 2014. Data are corrected for the effect of Earth tide and local atmospheric pressure. Gray: unfiltered data. Black: low-pass-filtered data (cutoff = 10 mHz).

a short interval (about two weeks), aimed at gaining insight into the characteristics of possible volcano-related mass redistribution.

4. Gravity Changes Driven by Volcanic Processes: Two Cases of Study

Past studies showed that volcano-related gravity changes do occur at Mount Etna, over a wide range of time scales (Carbone et al., 2017). Gravity changes of several tens of μGal were observed along the southern slope of the volcano, at elevations ranging between 1,500 and 2,000 m (Carbone et al., 2003a, 2003b). In contrast, most of the signal observed at SLN during the period covered in this study (October 2014–August 2017) is driven by groundwater mass changes (Figure 5a). Indeed, residuals after subtracting the estimated hydrological effect are within ±3 μGal (1σ confidence interval). Because of the high precision and long-term stability of iGrav meters (Warburton et al., 2010), interesting changes can be recognized in the residual signal from SLN, through comparison with (i) the signal from MNT and NIC and (ii) the other available information from the monitoring system of Mount Etna. To be able to set constraints on the characteristics of the mass sources behind the observed gravity changes, we consider data starting from July 2016, when iGrav#20 and iGrav#25 were installed at MNT and NIC, respectively (section 2). Indeed, data from a single site do not allow to make any inference on the position and characteristics of the mass source behind the observed gravity changes. Hence, for example, the gravity decrease (Figure 8) observed for nine days before the 28 December 2014 lava fountain from the New South-East Summit Crater (Bonforte & Guglielmino, 2015; Gambino et al., 2016) suggests that an underground mass decrease led the eruptive event, but not much can be said about the characteristics of the gravity source.

4.1. First Case Study: August–October 2016

The first case study involving data from the stations on Etna equipped with iGrav meters refers to the July–October 2016 interval, when the activity of Etna mainly consisted of continuous degassing from the summit craters. The signal from SLN during this period is shown in Figure 9 (top chart). Data are corrected for the effects of Earth tide and local atmospheric pressure and low-pass filtered (cutoff ≈ 0.01 Hz), to remove the higher-frequency component, mainly driven by ground shaking (volcanic tremor, local earthquakes, teleseismic events). We prefer not to apply the correction accounting for the effect of water-mass changes (section 3 and Figure 5a). Indeed, the best fitting hydrological model we derived using data from SLN mostly involves changes over periods longer than one month, while here we focus on shorter-term variations (period of up to 10 days).

Conversely, a low-rate (−0.04 μGal/day) linear trend is removed from the time series to better evidence the anomalies of interest. To account for other possible nonvolcanic effects (e.g., contribution of global atmospheric pressure variations to local gravity; Merriam, 1992), we subtract, from the gravity signal acquired at SLN, a component of the gravity signal acquired at NIC. Indeed, NIC is far enough from the active volcanic structures (Figure 1) and gravity changes driven by volcanic process at depth less than 10 km are not expected to induce measurable changes at NIC. Before being subtracted from the time series of SLN, data from NIC are band-pass filtered to remove (i) the higher-frequency (cutoff = 7 μHz; site and instrumental noise) and (ii) the longer-period (cutoff = 0.5 μHz; possible instrumental drift)

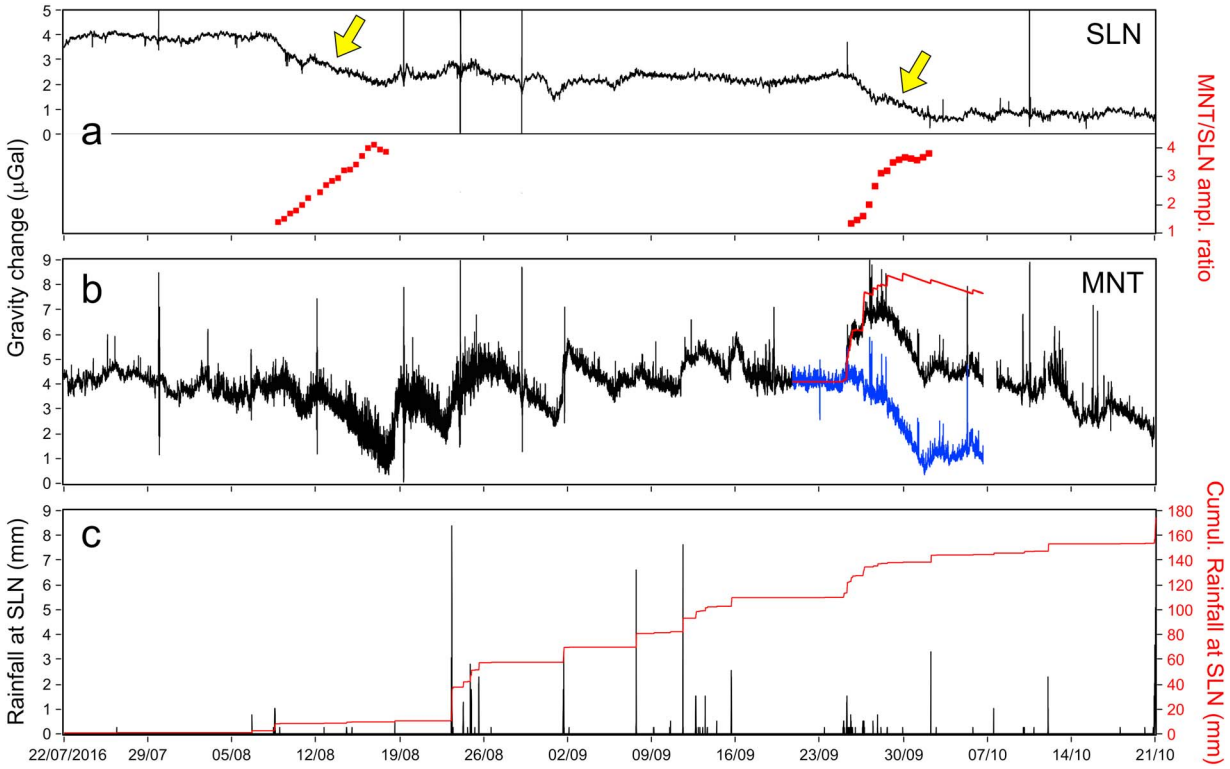

Figure 9. (a, top) Gravity time series from SLN during the 22 July to 21 October 2016 interval, corrected for the effect of Earth tide and local atmospheric pressure. A linear trend is removed from the time series that is also low-pass filtered (cutoff of 10 mHz). Furthermore, a component of the gravity signal acquired at NIC is subtracted from the data (see text for details). (bottom) MNT/SLN amplitude ratio calculated over a seven-day window sliding along the time series with a time step of 12 hr. (b) Black curve: gravity time series from MNT during the same time interval. The same data processing as before is applied, with the only exception that no linear trend is removed from the MNT time series. Red curve: model of the water-mass gravity effect during 17 September to 7 October (see text). Blue curve: MNT gravity data corrected for the water-mass effect (red curve). (c) Ten-minute precipitation rates and cumulative rainfall measured at SLN, during 22 July to 21 October 2016.

components. Filtering ensures that unwanted noise is not introduced in the signal from SLN. The residual time series is dominated by two negative changes (yellow arrows in Figure 9) occurring in early August and late September 2016. In both cases, the mean value of gravity decreases by up to 2 μGal, over intervals of less than 10 days.

The gravity signal from MNT during the same period is shown in middle chart of Figure 9. All the corrections applied to the signal from SLN (with the only exception of the low-rate linear trend) are also applied to the signal from MNT. While the first gravity decrease (first half of August) is clearly reproduced in the time series acquired at MNT, the second change (second half of September) is not evident, being masked by the short-term anomalies driven by rain events (bottom chart of Figure 9; see section 3). As discussed before, we do not consider it appropriate to derive a model of the gravity effect of water-mass changes for the entire time series recorded at MNT. Nevertheless, to gather information on the gravity source that induced the late September 2016 decrease, we tentatively calculate hydrological-driven effect on the signal from MNT during 17 September to 7 October (10 days). We again employ the formulation proposed by Crossley et al. (1998), but, diversely from the procedure we followed to derive the models of water-induced gravity effect at SLN and NIC (section 3), in this case the objective function is not of minimization type, but, rather, we aim at improving the correlation coefficient between the time series from MNT and SLN. Indeed, we aim at removing local effects from the MNT signal, thus retrieving volcano-driven changes common to both sites. Rain data from SLN (Figure 5e) are used as input to the computation. To account for possible differences between the amount of rain fallen during the same event at MNT and SLN, we apply a multiplicative coefficient to w (equation (1)), ranging between 0.5 and 2. This coefficient is automatically adjusted by the searching procedure for each rain event during the 10-day period.

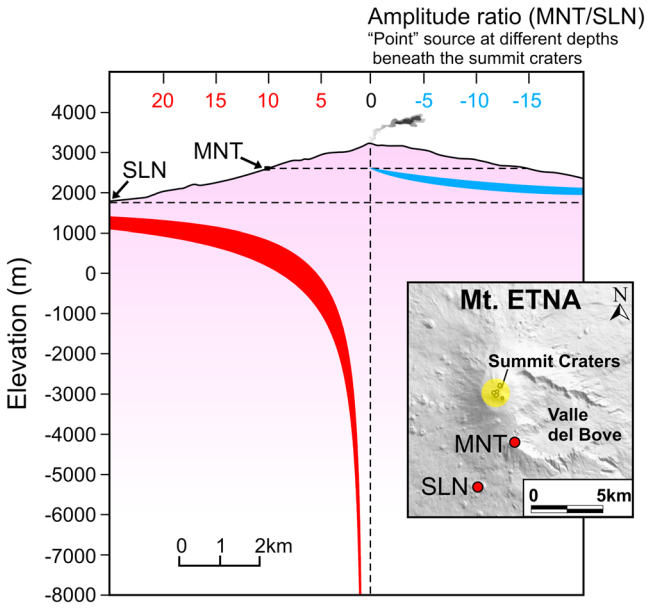

Figure 10. MNT/SLN gravity amplitude ratio versus depth of the mass source, assuming that the source features an almost spherical shape and that it lies beneath an ~2-km-wide area (yellow surface in the inset) enclosing the summit active craters of Etna. Note that our analysis identifies surfaces, rather than curves, since we are considering several possible horizontal positions of the source, implying that a range of possible depths, rather than a single value, is associated to each value of the amplitude ratio.

Results are shown in Figure 9 (middle chart). The most important differences between corrected (blue curve) and uncorrected (black curve) data are the removal of the two sudden changes on 25 and 26 September (slightly more and slightly less than 2 μGal, respectively, each occurring over periods of about 5 hr) that are almost entirely explained by the water-mass model. The latter (red curve in the middle chart of Figure 9) shows that the following water-induced gravity changes (until 7 October) are much smaller (within 1 μGal). The value of τ_1 found by the inversion scheme (about 16 min) indicates almost instantaneous infiltration of rain, thus confirming the major impact that water mass changes in the vadose zone may have on gravity changes observed at MNT (section 3). After MNT data during 17 September to 7 October are corrected for the effect of groundwater changes, we perform a cross-analysis using a seven-day window sliding along the time series from SLN and MNT with a time step of 12 hr. The analysis is restricted to two ~10-day subintervals encompassing the early-August and late-September gravity decreases. For each step of the window, we calculate correlation coefficient and amplitude ratio between MNT and SLN time series.

Results of the cross-analysis (red dots in the top chart of Figure 9) indicate that, in correspondence of each gravity decrease, the amplitude ratio between the gravity effects at MNT and SLN increases with time. As shown by Carbone et al. (2008) and Carbone and Poland (2012), the amplitude ratio between the signals from two observation points provides a constraint on the source location. In the case presented here, assuming that (i) the gravity source is almost unidimensional (e.g., can be considered a point source) and (ii) its horizontal position lies within a ~2-km-wide area enclosing the summit active craters of Etna, each value of the MNT/SLN amplitude ratio defines a range of possible source depths (Figure 10). The regular increase in the value of the amplitude ratio from about 1 to 4, coupled with the negative sign of the gravity changes observed at the two stations, indicates that, both in early August and late September, mass decreases occurred at increasingly shallow depths—starting at −5 km and rising to −2 km. Assuming that the mass source beneath the summit craters zone is centered in the middle of the depth range deduced from the amplitude ratio analysis, the values of the gravity changes observed at the two stations during both anomalous intervals are compatible with mass decreases on the order of 2×10^{10} kg, regardless the exact shape of the source itself. Indeed, given the relatively long source-to-sensor distances (7.5 to 9 km), the shape of the source has little influence on the amplitude of the required mass change, provided that (i) the maximum size of the source is within 3 km and (ii) its aspect ratio does not exceed ~10. The inferred mass changes, occurring over intervals of less than 10 days, would imply a magma flux much higher than the average supply rate of new magma at Etna ($70–250 \times 10^6$ m^3/year; Allard, 1997; Allard et al., 2006), for any plausible value of the density difference between newly arriving and gas-depleted magma. Hence, it is unlikely that the two observed gravity decreases are merely due to lighter magma batches rising along the plumbing system of Etna. Rather, our findings suggest a direct involvement of exsolved gas in the production of the two gravity changes. At Mount Etna, CO_2 is thought to become exsolved at considerable depth ($p > 200$ MPa; Moretti et al., 2018) and to flux the upward system, eventually accumulating in magma batches that evolve under closed-system conditions (Ferlito et al., 2014; Moretti et al., 2018). Hence, the two observed anomalies could reflect phases of bulk density decrease driven by increases in the gas/magma ratio at a depth of 2 to 5 km. Interestingly, this depth range is in keeping with the position of an intermediate storage zone, inferred through seismic (5 ± 2 km below sea level; Murru et al., 1999) and ground deformation data (Bonforte et al., 2008).

The inferred modifications of the density profile in the intermediate plumbing system of Etna are not associated to important changes in the state of activity of the volcano. However, it is worth noting that

- on 7 August, soon before the development of the first gravity anomaly, a new vent formed inside the Voragine summit crater that became the center of intense, pulsing degassing for several weeks;

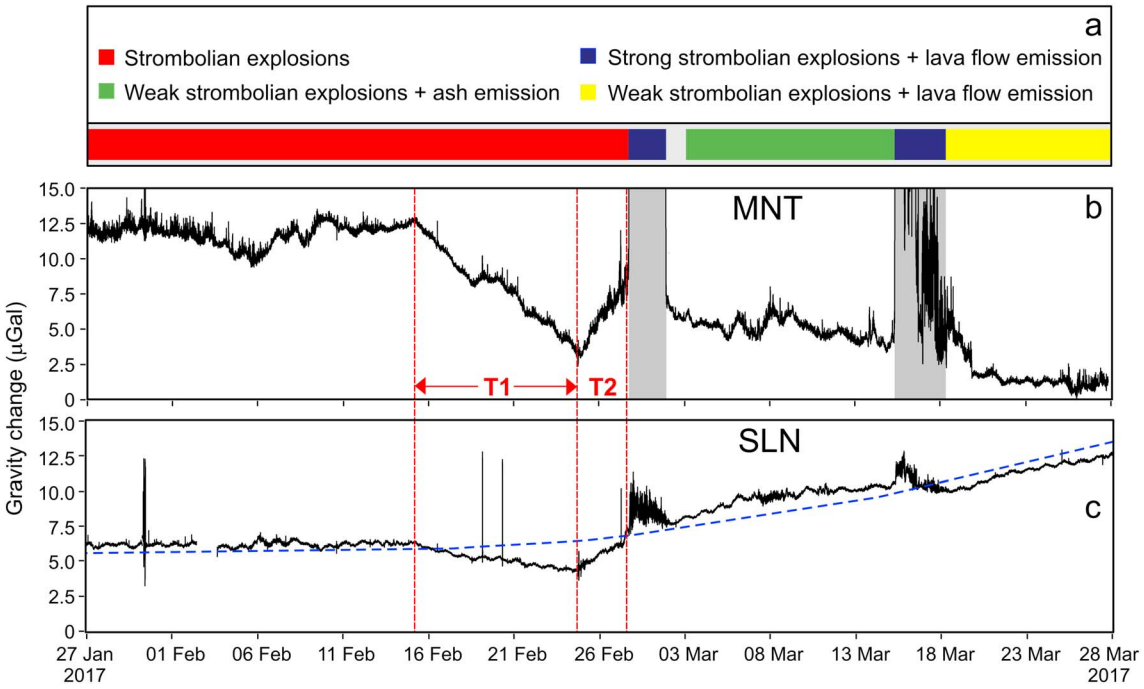

Figure 11. (a) Different phases of the volcanic activity during 27 January to 28 March 2017. (b) Gravity time series from MNT. Data are (i) corrected for the effect of Earth tide and local atmospheric pressure and (ii) low-pass filtered with cutoff of 10 mHz. Gray strips mark intervals where, due to severe ground shaking, gravity data are disregarded (see text for details). (c) Gravity time series from SLN (same corrections as in (b)). The dashed blue curve shows the gravity changes driven by underground water-mass redistributions (see section 3 and Figure 5a for details). Also in this case, a component of the contemporary gravity signal acquired at NIC is subtracted from the time series in (b) and (c).

- throughout August 2016, during and after the development of the first anomaly, mild explosive activity was observed at the Voragine summit crater, visible, during nightly hours, as gleams at the top of the volcano; and
- on 10 October, soon after the end of the second gravity decrease, a sequence of explosions occurred from the Bocca Nuova crater and the crater floor subsided by about 50 m.

The possible existence of a cause–effect link between the inferred mass decreases at intermediate depth and the above features of the activity of Etna during August to October 2016 is beyond the scope of the present paper. Here it is important to stress that spring gravimeters, almost exclusively used for measurements at volcanoes (Carbone et al., 2017), are not stable enough to observe the gravity changes presented here (a few μGal over intervals of ~10 days). Indeed, SGs are the only currently available gravimeters able to precisely describe the evolution of small gravity changes over time scales of days to months, and, thus, in the case of Etna, they are the only devices able to detect the inferred mass changes at intermediate depth. This ability is of uttermost importance, given the control that the underlying processes may exert on the eruptive activity of Etna (Ferlito et al., 2014).

4.2. Second Case Study: The Eruptive Phase at the Beginning of 2017

The second case study involves gravity data acquired during the eruptive phase at the beginning of 2017, from the Southeast Crater Complex (Figure 1). During early stages of this eruptive phase, weak Strombolian explosions and ash emission occurred from a new vent that opened in December 2016. Strong Strombolian activity and emission of lava flows from different vents in the Southeast Crater Complex occurred during later stages of the eruption (see Figure 11a). Between 15 and 24 February (T1; Figure 11), a negative gravity change was observed at both MNT and SLN. The amplitude of the change is much stronger at MNT than at SLN and the amplitude ratio (~5) points to a source at 0 to 1 km below the sea level (under the same assumptions as the previous case of study; Figure 10). The amount of mass decrease needed to explain the observations is on the order of 3.5×10^{10} kg. On 24 February, a reversal in the sign of the change is observed in both MNT and SLN time sequences. Indeed, an approximately three-

day (T2; Figure 11) gravity increase is observed, which leads to the phase of strong Strombolian activity and lava emission, starting on 27 February. While the value of the MNT/SLN amplitude ratio during T1 is well constrained, results during T2 are less straightforward due to its shorter duration and to the effect of volcano-related ground shaking, especially on the signal from MNT (see Figure 11b and section 2). However, within the above limits, the value of the amplitude ratio seems to be lower during T2, than during T1. Under the assumption that only a (unidimensional) mass source was active during T2, a lower MNT/SLN amplitude ratio implies a deeper mass source than during T1 (Figure 10). Nevertheless, it is unlikely that a deepening of the mass source may have led to a more intense phase of the eruption. An alternative possibility is that the gravity increase during T2 reflects a more complex process, involving mass changes at different depths. For example, a transfer of lighter mass toward shallower depths, implying (i) a mass increase in the same source volume where changes occurred during T1 and (ii) a mass decrease at shallower depth, would result in a value of the amplitude ratio lower than expected if only the deeper change occurred. In particular, we calculated that the cumulative effect of a mass increase and decrease occurring (i) 0 to 1 km below sea level and (ii) around 1 km asl, respectively, could explain the MNT/SLN amplitude ratio observed during T2. The amplitude of the changes at the two stations points to an amount of mass increase and decrease in the two source volumes, both near to the amount of mass change inferred to have occurred during T1 (3.5×10^{10} kg).

The above observations would suggest that the pattern of gravity changes observed at the two gravity stations between 15 and 27 February 2017 involves (i) accumulation of gas phase at 0–1 km below sea level (T1) and (ii) subsequent transfer of the gas phase/gas-rich magma toward shallower levels of the feeding system (T2), soon before the start of the intense phase of the eruption. Successively (since the beginning of March), a different evolution is observed in the signal from the two stations: while at SLN a gravity increase is observed that continues, at a decreasing rate, until the end of the considered interval, a slight decrease occurs at MNT. Important hydrological effects were inferred to occur at SLN, especially during the second part of the studied period (dashed blue curve in Figure 11c). They were mainly driven by the melting of snow (Figures 5a and 5d) and are, at least in part, responsible for the increase observed since the end of February 2017.

5. Concluding Remarks

In most cases, continuous gravity measurements at volcanoes are performed using spring gravimeters, which are easily portable and do not require much power, thus allowing deployment at remote field locations (e.g., close to active craters; Carbone et al., 2015; Poland & Carbone, 2016). Unfortunately, these instruments are influenced by environmental factors and are subject to instrumental drift; hence, when used in continuous mode for interval longer than about 10 days, they do not provide reliable measurements (Carbone et al., 2017).

Here we show that, thanks to negligible instrumental drift and lack of instrumental artifacts due to ambient parameters, iGrav SGs allow detection of gravity changes as small as 2 μGal and less, over a wide range of periods. Only instruments with such detection power can identify the weak gravity signature of changes in the gas/magma ratio occurring at intermediate depth in the plumbing system of Etna during noneruptive intervals (see section 4.1). Given the implications that the buildup of gas at various levels may have on the onset of eruptive phases at Etna (Moretti et al., 2018), the ability to precisely describe the evolution of mass changes at intermediate depth is of uttermost importance and fully justifies the use of iGrav meters. That holds even though, due to intrinsic limitations (high power consumption, need of a large footprint), iGrav SGs cannot be installed in the vicinity of active volcanic structures, where there is the maximum chance of measuring the largest volcano-related gravity changes.

Three iGra versus operating on Etna since 2016 demonstrate two substantial advantages of a mini-array compared to a single instrument. First, the mini-array permits to discriminate nonvolcanic from volcanic gravity effects, through comparison of the signals from the innermost stations (MNT and SLN) with the signal from the outermost station (NIC). Second, cross-analysis of the signals from MNT and SLN sets constraints on the position (mainly depth) of volcano-related gravity sources (see previous section and Figure 10). Indeed, the different MNT/SLN amplitude ratios found in the two above case studies (sections 4.1 and 4.2) strongly suggests the activation of mass sources at different levels throughout the plumbing system of Etna. Shallower mass redistributions, like the ones inferred to (i) have preceded the onset of most lava fountains during the sequence of eruptive events in the summer of 2011 (Carbone et al., 2015) and (ii) have

been produced by magma intrusion along the South rift zone during October 1995 to July 1996 (Budetta et al., 1999), would result in higher values of the MNT/SLN amplitude ratio, or even a measurable effect only at MNT station.

To unequivocally identify the gravity signature of volcanic processes, great care must be paid to recognize the effects induced by changes in groundwater mass. Indeed, using a nearly three-year time series from SLN, together with meteorological information, we show that most of the observed gravity changes, over time scales longer than about one month, are driven by hydrological processes (section 3 and Figure 5a). At MNT, a combination of topographic and geological conditions dictates that fast (time scales of a few hours to a few days) and relatively strong (several μGal) gravity changes may develop almost simultaneously with rainfall events (Figures 5b and 6). The same events do not induce measurable gravity changes over the same time scale at SLN, or induce change much smaller than at MNT (see section 3 and Figure 6). Hence, if the rainfall data were disregarded, one could erroneously deduce that the sudden changes at MNT are due to volcanic processes occurring at shallow depth. These observations clearly demonstrate the need to equip MNT (as well as the other sites on Etna hosting iGravs) with meteorological sensors furnishing as much high-quality information as possible on the evolution of the local water balance. That would allow development of an accurate model of the gravity effect induced by changes in the groundwater mass, thus retrieving unambiguously the anomalies likely due to volcanic processes.

Our pioneering long-term use of iGra versus at an active volcano highlights a shortcoming of these devices: long-period volcano seismicity (strong LP events and high-amplitude volcanic tremor) may induce fictitious positive changes in the average level of the gravity signal (section 2). Therefore, during the paroxysmal phases of explosive eruption events, information from iGrav meters (Figures 4 and 11b) is missed, unless they are far enough from the active centers where, however, volcano-related gravity changes may be too small to detect. A similar behavior was observed for continuously running spring gravimeter (Carbone et al., 2015). It is important to properly recognize the parts of the signal from iGrav meters that are affected by the above shortcoming, not to incur in erroneous conclusions on the characteristics of the underlying bulk mass redistributions. We are running tests aimed at understanding whether compensating algorithms can be developed to remove the instrumental effect of ground shaking from the signal of iGrav SGs. Alternative solutions include (i) modifying the magnetic support system of the iGrav to dramatically increase the horizontal restoring force on the sphere or (ii) operating the iGrav on an isolation system that attenuates horizontal vibrations from long-period volcano seismicity to an acceptable level.

Apart from the limits discussed above, our study proves that iGrav SGs are powerful tools to monitor and study active volcanoes and can provide unique information on the amount and time evolution of mass changes occurring at different levels throughout the magma feeding system. Hence, especially if used in the framework of a multiparameter monitoring system, they have the potential to improve our knowledge of how volcanoes work.

Acknowledgments

We are indebted to A. Messina for his continued support in managing the mini-array of iGrav SGs at Mount Etna and handling the gravity data. We are grateful to the INGV technicians that manage and maintain the GPS permanent network of Etna and to G. Leto and P. Bruno, from the Italian National Institute for Astrophysics (INAF), who provided meteorological data from SLN station. Thanks are also due to P. Tregoning and two anonymous reviewers for their thorough evaluations of our manuscript. This research was partially supported by the H2020 NEWTON-g project (Grant Agreement 801221). All gravity data presented in this paper are publicly available at https://doi.org/10.5281/zenodo.2416536.

References

Allard, P. (1997). Endogenous magma degassing and storage at Mount Etna. *Geophysical Research Letters*, *24*(17), 2219–2222. https://doi.org/10.1029/97GL02101

Allard, P., Behncke, B., D'Amico, S., Neri, M., & Gambino, S. (2006). Mount Etna 1993–2005: Anatomy of an evolving eruptive cycle. *Earth-Science Reviews*, *78*(1-2), 85–114. https://doi.org/10.1016/j.earscirev.2006.04.002

Andò, B., & Carbone, D. (2004). A test on a neuro-fuzzy algorithm used to reduce continuous gravity records for the effect of meteorological parameters. *Physics of the Earth and Planetary Interiors*, *142*(1–2), 37–47. https://doi.org/10.1016/j.pepi.2003.12.006

Battaglia, M., Gottsmann, J., Carbone, D., & Fernández, J. (2008). 4D volcano gravimetry. *Geophysics*, *73*(6), WA3–WA18. https://doi.org/10.1190/1.2977792

Battaglia, M., Segall, P., & Roberts, C. (2003). The mechanics of unrest at Long Valley caldera, California. 2. Constraining the nature of the source using geodetic and microgravity data. *Journal of Volcanology and Geothermal Research*, *127*(3–4), 219–245. https://doi.org/10.1016/S0377-0273(03)00171-9

Battaglia, M., Troise, C., Obrizzo, F., Pingue, F., & De Natale, G. (2006). Evidence for fluid migration as the source of deformation at Campi Flegrei caldera (Italy). *Geophysical Research Letters*, *33*, L01307. https://doi.org/10.1029/2005GL024904

Bonforte, A., Bonaccorso, A., Guglielmino, F., Palano, M., & Puglisi, G. (2008). Feeding system and magma storage beneath Mt Etna as revealed by recent inflation/deflation cycles. *Journal of Geophysical Research*, *113*, B05456. https://doi.org/10.1029/2007JB005334

Bonforte, A., & Guglielmino, F. (2015). Very shallow dyke intrusion and potential slope failure imaged by ground deformation: The 28 December 2014 eruption on Mount Etna. *Geophysical Research Letters*, *42*, 2727–2733. https://doi.org/10.1002/2015GL063462

Branca, S., Carbone, D., & Greco, F. (2003). Intrusive mechanism of the 2002 NE-Rift eruption at Mt. Etna (Italy) inferred through continuous microgravity data and volcanological evidences. *Geophysical Research Letters*, *30*(20), L06305. https://doi.org/10.1029/2003GL018250

Budetta, G., Carbone, D., & Greco, F. (1999). Subsurface mass redistribution at Mount Etna (Italy) during the 1995–96 explosive activity detected by microgravity studies. *Geophysical Journal International*, *138*(1), 77–88. https://doi.org/10.1046/j.1365-246x.1999.00836.x

Carbone, D., Budetta, G., & Greco, F. (2003a). Bulk processes prior to the 2001 Mount Etna eruption, highlighted through microgravity studies. *Journal of Geophysical Research*, *108*(B12), 2556. https://doi.org/10.1029/2003JB002542

Carbone, D., Budetta, G., & Greco, F. (2003b). Possible mechanisms of magma redistribution under Mt. Etna during the 1994–1999 period detected through microgravity measurements. *Geophysical Journal International*, *153*(1), 187–200. https://doi.org/10.1046/j.1365-246X.2003.01901.x

Carbone, D., Poland, M. P., Diament, M., & Greco, F. (2017). The added value of time-variable microgravimetry to the understanding of how volcanoes work. *Earth-Science Reviews*, *169*, 146–179. https://doi.org/10.1016/j.earscirev.2017.04.014

Carbone, D., Jousset, P., & Musumeci, C. (2009). Gravity "steps" at Mt. Etna volcano (Italy): Instrumental effects or evidences of earthquake-triggered magma density changes? *Geophysical Research Letters*, *36*, L02301. https://doi.org/10.1029/2008GL0361

Carbone, D., & Poland, M. P. (2012). Gravity fluctuations induced by magma convection at Kīlauea Volcano, Hawai'i. *Geology*, *40*(9), 803–806. https://doi.org/10.1130/G33060.1

Carbone, D., Poland, M. P., Patrick, M. R., & Orr, T. R. (2013). Continuous gravity measurements reveal a low-density lava lake at Kīlauea Volcano, Hawai'i. *Earth and Planetary Science Letters*, *376*, 178–185. https://doi.org/10.1016/j.epsl.2013.06.024

Carbone, D., Zuccarello, L., Messina, A., Scollo, S., & Rymer, H. (2015). Balancing bulk gas accumulation and gas output before and during lava fountaining episodes at Mt. Etna. *Scientific Reports*, *5*(1), 18,049. https://doi.org/10.1038/srep18049

Carbone, D., Zuccarello, L., Montalto, P., & Rymer, H. (2012). New geophysical insight into the dynamics of Stromboli volcano (Italy). *Gondwana Research*, *22*(1), 290–299. https://doi.org/10.1016/j.gr.2011.09.007

Carbone, D., Zuccarello, L., & Saccorotti, G. (2008). Geophysical indications of magma uprising at Mt. Etna during the December 2005 to January 2006 non-eruptive period. *Geophysical Research Letters*, *35*, L06305. https://doi.org/10.1029/2008GL033212

Carbone, D., Zuccarello, L., Saccorotti, G., & Greco, F. (2006). Analysis of simultaneous gravity and tremor anomalies observed during the 2002–2003 Etna eruption. *Earth and Planetary Science Letters*, *245*(3-4), 616–629. https://doi.org/10.1016/j.epsl.2006.03.055

Carbone, D., Zuccarello, L., Saccorotti, G., Rymer, H., & Rapisarda, S. (2010). The effect of inertial accelerations on the higher frequency components of the signal from spring gravimeters. *Geophysical Journal International*, *182*(2), 772–780. https://doi.org/10.1111/j.1365-246X.2010.04644.x

Creutzfeldt, B., Güntner, A., Klügel, T., & Wziontek, H. (2008). Simulating the influence of water storage changes on the superconducting gravimeter of the Geodetic Observatory Wettzell, Germany. *Geophysics*, *73*(6), WA95–WA104. https://doi.org/10.1190/1.2992508

Crossley, D., Xu, S., & Van Dam, T. (1998).Comprehensive analysis of 2 years of SG data from Table Mountain, Colorado. Paper presented at 13th international symposium on Earth tides, Brussels (pp. 659–668).

Deville, S., Jacob, T., Chery, J., & Champollion, C. (2013). On the impact of topography and building mask on time varying gravity due to local hydrology. *Geophysical Journal International*, *192*, 82–93. https://doi.org/10.1093/gji/ggs007

Ferlito, C., Coltorti, M., Lanzafame, G., & Giacomoni, P. P. (2014). The volatile flushing triggers eruptions at open conduit volcanoes: Evidence from Mount Etna volcano (Italy). *Lithos*, *184*, 447–455. https://doi.org/10.1016/j.lithos.2013.10.030

Gambino, S., Cannata, A., Cannavò, F., La Spina, A., Palano, M., Sciotto, M., et al. (2016). The unusual 28 December 2014 dike-fed paroxysm at Mount Etna: Timing and mechanism from a multidisciplinary perspective. *Journal of Geophysical Research: Solid Earth*, *121*, 2037–2053. https://doi.org/10.1002/2015JB012379

Goodkind, J. M. (1999). The superconducting gravimeter. *Review of Scientific Instruments*, *70*(11), 4131–4152. https://doi.org/10.1063/1.1150092

Gottsmann, J., Carniel, R., Coppo, N., Wooller, L., Hautmann, S., & Rymer, H. (2007). Oscillations in hydrothermal systems as a source of periodic unrest at caldera volcanoes: Multiparameter insights from Nisyros, Greece. *Geophysical Research Letters*, *34*, L07307. https://doi.org/10.1029/2007GL029594

Güntner, A., Reich, M., Mikolaj, M., Creutzfeldt, B., Schroeder, S., & Wziontek, H. (2017). Landscape-scale water balance monitoring with an iGrav superconducting gravimeter in a field enclosure. *Hydrology and Earth System Sciences*, *21*(6), 3167–3182. https://doi.org/10.5194/hess-21-3167-2017

Hemmings, B., Gottsmann, J., Whitaker, F., & Coco, A. (2016). Investigating hydrological contributions to volcano monitoring signals. A time-lapse gravity example. *Geophysical Journal International*, *207*(1), 259–273. https://doi.org/10.1093/gji/ggw266

Hinderer, J., Crossley, D., & Warburton, R. J. (2015). 3.04—Superconducting gravimetry. In G. Schubert (Ed.), *Treatise on Geophysics* (2nd ed., pp. 59–115). Oxford: Elsevier. https://doi.org/10.1016/B978-0-444-53802-4.00062-2

Judson, A., & Doesken, N. (2000). Density of freshly fallen snow in the central Rocky Mountains. *Bulletin of the American Meteorological Society*, *81*(7), 1577–1587. https://doi.org/10.1175/1520-0477(2000)081<1577:DOFFSI>2.3.CO;2

Larson, K. M., & Nievinski, F. G. (2013). GPS snow sensing: Results from the EarthScope plate boundary observatory. *GPS Solutions*, *17*(1), 41–52. https://doi.org/10.1007/s10291-012-0259-7

Merriam, J. B. (1992). Atmospheric pressure and gravity. *Geophysical Journal International*, *109*(3), 488–500. https://doi.org/10.1111/j.1365-246X.1992.tb00112.x

Moretti, R., Métrich, N., Arienzo, I., Di Renzo, V., Aiuppa, A., & Allard, P. (2018). Degassing vs. eruptive styles at Mt. Etna volcano (Sicily, Italy). Part I: Volatile stocking, gas fluxing, and the shift from low-energy to highly explosive basaltic eruptions. *Chemical Geology*, *482*, 1–17. https://doi.org/10.1016/j.chemgeo.2017.09.017

Mouyen, M., Fong Chao, B., Hwang, C., & Hsieh, W. (2016). Gravity monitoring of Tatun volcanic group activities and inference for underground fluid circulations. *Journal of Volcanology and Geothermal Research*, *328*, 45–58. https://doi.org/10.1016/j.jvolgeores.2016.10.001

Murru, M., Montuori, C., Wyss, M., & Privitera, E. (1999). The locations of magma chambers at Mt. Etna, Italy, mapped by *b* values. *Geophysical Research Letters*, *26*(16), 2553–2556. https://doi.org/10.1029/1999GL900568

Peterson, J. (1993). Observations and modelling of seismic background noise, *U.S. Geol. Surv. Open-File Report*, 93–332. https://doi.org/10.3133/ofr93322

Poland, M. P., & Carbone, D. (2016). Insights into shallow magmatic processes at Kīlauea Volcano, Hawai'i, from a multiyear continuous gravity time series. *Journal of Geophysical Research: Solid Earth*, *121*, 5477–5492. https://doi.org/10.1002/2016JB013057

Poland, M. P., & Carbone, D. (2018). Continuous gravity and tilt reveal anomalous pressure and density changes associated with gas pistoning within the summit lava Lake of Kīlauea Volcano, Hawai'i. *Geophysical Research Letters*, *45*(5), 2319–2327. https://doi.org/10.1002/2017GL076936

Rosat, S., & Hinderer, J. (2018). Limits of detection of gravimetric signals on Earth. *Scientific Reports*, *8*(1), 15324. https://doi.org/10.1038/s41598-018-33717-z

Sainz-Maza Aparicio, S., Arnoso Sampedro, J., González Montesinos, F., & Martí Molist, J. (2014). Volcanic signatures in time gravity variations during the volcanic unrest on El Hierro (Canary Islands). *Journal of Geophysical Research: Solid Earth*, *119*, 5033–5051. https://doi.org/10.1002/2013JB010795

Tilling, R. I. (2008). The critical role of volcano monitoring in risk reduction. *Advances in Geosciences*, *14*, 3–11. https://doi.org/10.5194/adgeo-14-3-2008

Van Camp, M., de Viron, O., Pajot-Métivier, G., Casenave, F., Watlet, A., Dassargues, A., & Vanclooster, M. (2016). Direct measurement of evapotranspiration from a forest using a superconducting gravimeter. *Geophysical Research Letters*, *43*, 10,225–10,231. https://doi.org/10.1002/2016GL070534

Van Camp, M., de Viron, O., Watlet, A., Meurers, B., Francis, O., & Caudron, C. (2017). Geophysics from terrestrial time-variable gravity measurements. *Reviews of Geophysics*, *55*, 938–992. https://doi.org/10.1002/2017RG000566

Waltz, R. A., Morales, J. L., Nocedal, J., & Orban, D. (2006). An interior algorithm for nonlinear optimization that combines line search and trust region steps. *Mathematical Programming*, *107*(3), 391–408. https://doi.org/10.1007/s10107-004-0560-5

Warburton, R. L., Pillai, H. & Reineman, R. C. (2010). Initial results with the new GWR iGrav™ superconducting gravity meter. Paper Presented at: IAG Symposium on Terrestrial Gravimetry: Static and Mobile Measurements (TG-SMM2010), Saint Petersburg, Russia.

Wenzel, H. G. (1996). The nanogal software: Earth tide data processing package ETERNA 3.30. *Bulletin d'Informations des Marées Terrestres*, *124*, 9425–9439.